

Enzymatic and structural insights for substrate specificity of a family of jumonji histone lysine demethylases

John R Horton^{1,4}, Anup K Upadhyay^{1,4}, Hank H Qi^{2,3,4}, Xing Zhang¹, Yang Shi^{2,3} & Xiaodong Cheng¹

Combinatorial readout of multiple covalent histone modifications is poorly understood. We provide insights into how an activating histone mark, in combination with linked repressive marks, is differentially ‘read’ by two related human demethylases, PHF8 and KIAA1718 (also known as JHDM1D). Both enzymes harbor a plant homeodomain (PHD) that binds Lys4-trimethylated histone 3 (H3K4me3) and a jumonji domain that demethylates either H3K9me2 or H3K27me2. The presence of H3K4me3 on the same peptide as H3K9me2 makes the doubly methylated peptide a markedly better substrate of PHF8, whereas the presence of H3K4me3 has the opposite effect, diminishing the H3K9me2 demethylase activity of KIAA1718 without adversely affecting its H3K27me2 activity. The difference in substrate specificity between the two is explained by PHF8 adopting a bent conformation, allowing each of its domains to engage its respective target, whereas KIAA1718 adopts an extended conformation, which prevents its access to H3K9me2 by its jumonji domain when its PHD engages H3K4me3.

The control of gene expression in eukaryotes relies in part on the methylation status of histone proteins. Histone lysine modification is a dynamic process established by specific methyltransferases, including SET-domain proteins¹ and a conventional methyltransferase-like protein Dot1 (ref. 2). These methylation marks can be ‘erased’ by protein lysine demethylases that include flavin-dependent monoamine oxidase LSD1 (ref. 3) and α -ketoglutarate-Fe²⁺-dependent dioxygenases containing jumonji domains^{4–6}. Protein modules, such as PHD finger protein (PHFs), detect the methylation status of histones by recognizing lysine in methylated^{7–10} and unmethylated states^{11,12}. The jumonji domain often associates with at least one additional recognizable protein domain within the same polypeptide¹³. For example, JMJD2A contains an N-terminal jumonji domain and C-terminal PHD and tudor domains. The JMJD2A jumonji domain alone is capable of demethylating tri- (H3K9me3) and dimethylated histone H3 Lys9 (H3K9me2) and tri- (H3K36me3) and dimethylated Lys36 (H3K36me2), though it does so with a very low turnover rate ($k_{\text{cat}} < 1 \text{ h}^{-1}$ and $k_{\text{cat}}/K_{\text{M}} \sim 0.01 \text{ h}^{-1} \mu\text{mol}^{-1}$) (ref. 14).

Structural studies revealed that the JMJD2A jumonji domain predominantly recognizes the backbone of the histone peptides (unusually for a sequence-specific enzyme), allowing the enzyme to demethylate both H3K9me3 and H3K9me2 as well as H3K36me3 and H3K36me2 (refs. 14–16). Meanwhile, the JMJD2A tudor domain binds two different histone sequences (H3K4me3 and H4K20me3) via radically different approaches^{17,18}. The functional connection between the methyl mark reader and eraser in JMJD2A is not clear. Here, we ask whether regions outside of the catalytic core domain influence the specificity and/or efficiency of the catalytic domain, as in the case of DNA methyltransferase 1 (refs. 19,20), and we explore this possibility in the context of PHF8 and KIAA1718.

PHF8 and KIAA1718 belong to a small family of jumonji proteins with three members in mice and humans (PHF2, PHF8 and KIAA1718) (ref. 13). Each of these proteins harbors two domains in its respective N-terminal half (Fig. 1a): a PHD domain that binds H3K4me3 and a jumonji domain that demethylates H3K9me2, H3K27me2 and H3K36me2 (ref. 21) (see below). The two proteins share 82% identity (87% similarity) between their PHDs and 64% identity (75% similarity) between their jumonji domains (Supplementary Fig. 1). Mutations in the jumonji domain of human PHF8—either deletions or a missense mutation (F279S)—cause inherited X-linked mental retardation^{21–24}. Relative to PHF8, KIAA1718 has a 30-residue alanine-rich addition followed by a stretch of 6 prolines in the N terminus, and a 3-residue insertion in the nonconserved linker between PHD and jumonji domains (Supplementary Fig. 1). The sequence and length of the linker of KIAA1718 are highly conserved among the orthologs from different species, whereas the corresponding linker of PHF8 varies in sequence (it contains more glycines) and length (it is often shorter, between 11 and 15 residues) (Supplementary Fig. 2). Here, we focus on residues 1–488 from KIAA1718 and residues 1–447 from PHF8, comparing their demethylase activities on dimethylated lysine at H3K9 (H3K9me2) or H3K27 (H3K27me2) and analyzing the effect of trimethylation of H3K4 (H3K4me3) on demethylation activity.

RESULTS

H3K4me3 binding by the PHF8 PHD enhances demethylation

PHF8, containing both the PHD and jumonji domains (Fig. 1a), has slow activity on H3_{1–24}K9me2, with $t_{1/2}$ (the time required for 50% demethylation under the assay conditions) of $\sim 1 \text{ h}$ (Fig. 1b, top left). We probed the demethylation activity of PHF8 on a histone H3

¹Department of Biochemistry, Emory University School of Medicine, Atlanta, Georgia, USA. ²Department of Pathology, Harvard Medical School, Boston, Massachusetts, USA. ³Division of Newborn Medicine, Department of Medicine, Children’s Hospital, Boston, Massachusetts, USA. ⁴These authors contributed equally to this work. Correspondence should be addressed to X.C. (xcheng@emory.edu).

Received 29 October; accepted 1 December; published online 20 December 2009; doi:10.1038/nsmb.1753

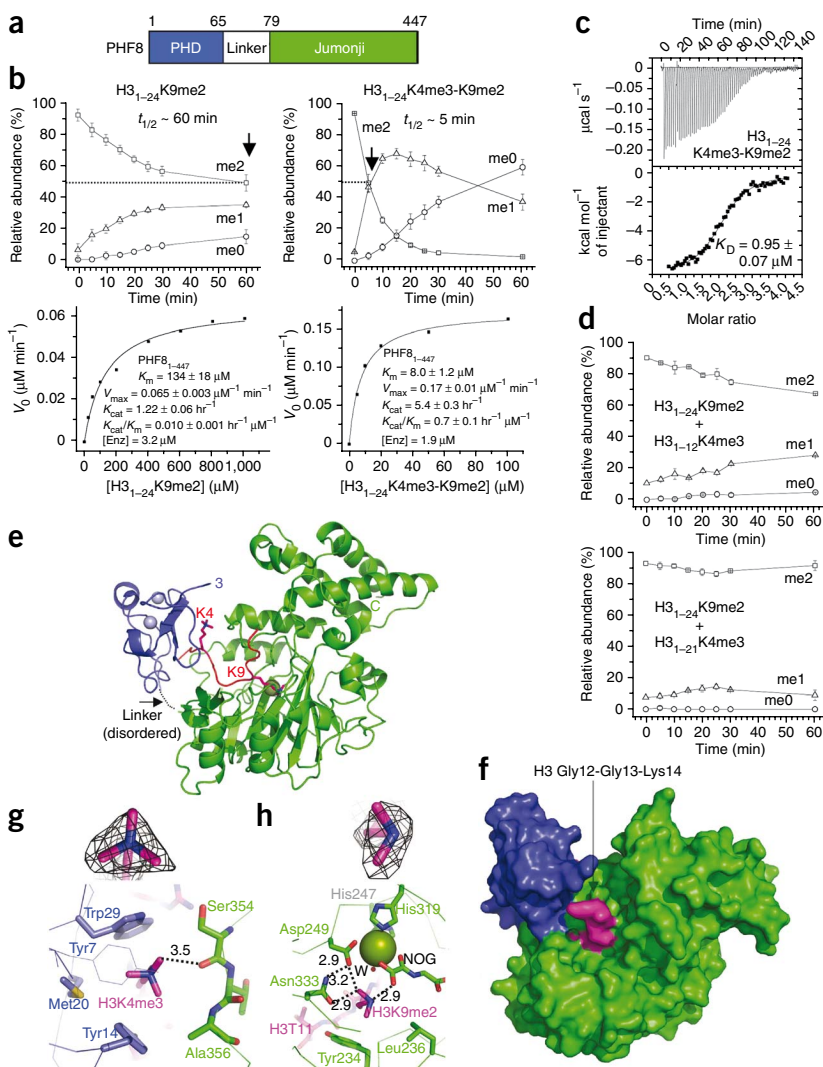
Figure 1 PHF8 PHD domain binding of H3K4me3 enhances its jumonji domain-mediated demethylation of H3K9me2.

(a) Schematic representation of PHF8. (b) Effect of H3K4me3 on the demethylation of H3K9me2 by PHF8. Top panels show progression of demethylation as a function of reaction time. **Supplementary Figure 11a** shows representative mass spectra at various time points. Bottom panels show kinetics of PHF8 on two peptide substrates, with calculated kinetic parameters. (c) ITC measurement of binding of PHF8 to doubly methylated H3₁₋₂₄K4me3-K9me2 peptides, carried out under the conditions of 11 μM protein concentration and 0.2 mM peptide concentration in 100 mM NaCl and 50 mM HEPES, pH 7.0. (d) The inhibitory effect of adding an equimolar ratio of H3₁₋₁₂K4me3 (top) or H3₁₋₂₁K4me3 peptides (bottom) on the demethylation of H3₁₋₂₄K9me2 by PHF8. (e) The PHD (blue) and jumonji (green) collaborate in binding the H3 peptide (magenta) containing H3K4me3 and H3K9me2. Omit electron densities, $F_o - F_c$ (black mesh), contoured at 4σ above the mean, are shown for the trimethylated H3K4me3 and dimethylated H3K9me2, respectively. (f) The surface representation of PHF8, colored with blue (PHD), green (jumonji) and magenta (H3 peptide). (g) H3K4me3 binding in the cage, surrounded on four sides by Tyr14, Met20 and Trp29 of PHD (blue) and Ser354 of jumonji (green). The carbonyl oxygen of Ser354 is in van der Waals contact with one of the methyl groups. Tyr7 (in thin lines) covers the top of the cage. (h) H3K9me2 binds in the active site.

peptide modified with both H3K4me3 and H3K9me2. The presence of H3K4me3 enhanced PHF8 activity on H3K9me2 by 12-fold, with $t_{1/2} \sim 5$ min (**Fig. 1b**, top right). PHF8 has lower K_M by a factor of 16 and higher k_{cat} by a factor of 4 on the doubly methylated peptide than that of H3K9me2 peptide (**Fig. 1b**, lower panels). In addition, PHF8 binds the doubly methylated peptide with a K_D of approximately 1 μM (**Fig. 1c**), whereas it has negligible binding on H3₁₋₂₄K9me2 under the conditions tested (data not shown). In contrast, when present in *trans*, the H3K4me3 modification either in a short H3₁₋₁₂ or a long H3₁₋₂₁ peptide inhibits the PHF8 activity on H3₁₋₂₄K9me2 (**Fig. 1d**).

To understand how H3K4me3 binding enhances demethylase activity, we determined the cocrystal structure of PHF8₁₋₄₄₇ with an H3₁₋₂₄ peptide containing H3K4me3 and H3K9me2 (**Fig. 1e**) in the presence of Fe^{2+} and *N*-oxalylglycine (the cofactor analog) to form a catalytically inert complex (**Table 1**). The structure, determined at a resolution of 2.2 Å, shows that the PHD and jumonji domains act in concert in substrate recognition. The first 11 residues of the H3 peptide were nearly buried in a deep cleft between the PHD and the jumonji domains with a disordered linker (residues 66–78) (**Fig. 1e**). The H3 N terminus was buried in the PHD-jumonji interface, and Gly12-Gly13-Lys14 emerged from an opening on the surface of the jumonji domain (**Fig. 1f**); the remainder of the peptide (residues 15–24) was unstructured.

The limited solvent exposure of bound histone peptide implies that the substrate did not diffuse into a preformed binding site. The surface area buried at the PHF8-peptide interface is approximately



1,550 Å² (with ~30% contribution from the PHD and ~70% from the jumonji domain). The H3 peptide shows an extended conformation from Ala1 to Lys9, then makes a sharp, nearly 90° turn at Lys9 (**Fig. 1e** and **Supplementary Fig. 3a**). Besides main chain interactions, all 11 side chains of H3 (Ala1–Thr11) are involved in interactions, either with both domains (Ala1, Arg2, Lys4me3 (K4me3), Thr6; **Supplementary Fig. 3b–e**), PHD alone (Thr3) or jumonji alone (Gln5 and Ala7–Thr11; **Supplementary Fig. 3f–i**). Intramolecular interactions occur between Thr3 and Gln5 (**Supplementary Fig. 3f**) and Arg8 and Ala7 (**Supplementary Fig. 3g**). This is in sharp contrast to the structures of JMJD2A jumonji domains in complex with substrate peptides that have little side chain contact^{14–16}.

Substrate specificity is contributed by both domains, as exemplified by the interactions of H3K4me3 with PHD (through the hydrophobic cage) and jumonji (through a van der Waals contact with the main chain carbonyl oxygen of Ser354) (**Fig. 1g**). The target K9me2 lies in the active site right next to the Fe^{2+} and *N*-oxalylglycine (**Fig. 1h**). One of its terminal *N*-CH₃ groups projects toward the aromatic ring of Tyr234, and the other methyl group points toward Asp249 and Asn333, forming two hydrogen bonds of C–H–O type (**Fig. 1h**)—a type of hydrogen bond that occurs in the active sites of both SET and jumonji domains^{14,25}. The dimethylated terminal nitrogen atom carrying the lone pair of electrons forms a hydrogen bond with one of the oxygen atoms of

Table 1 Data collection and refinement statistics (molecular replacement)

Data collection	PHF8 (residues 1-447)	KIAA1718 (residues 1-488)		KIAA1718 (residues 92-488)		
Cofactors	Zn ²⁺ , Fe ²⁺ , <i>N</i> -oxalylglycine	Zn ²⁺ , Fe ²⁺ , <i>N</i> -oxalylglycine	Zn ²⁺ , Fe ²⁺ , α -ketoglutarate	Fe ²⁺	Fe ²⁺ , α -ketoglutarate	Fe ²⁺ , <i>N</i> -oxalylglycine
Peptide	H3(1–24)K4me3-K9me2					
Space group	P4 ₃ 2 ₁ 2		P2 ₁ 2 ₁ 2 ₁		P6 ₁ 22	
Cell dimensions	$(\alpha = \beta = \gamma = 90^\circ)$		$(\alpha = \beta = \gamma = 90^\circ)$		$(\alpha = \beta = 90^\circ, \gamma = 120^\circ)$	
<i>a</i> , <i>b</i> , <i>c</i> (Å)	73.5, 73.5, 210.8	62.7, 125.6, 206.1	63.4, 125.2, 206.0	77.9, 77.9, 289.7	78.1, 78.1, 290.8	78.3, 78.3, 289.1
Resolution (Å)	34.72–2.19 (2.27–2.19) ^a	34.82–2.39 (2.48–2.39)	34.54–2.89 (2.99–2.89)	34.32–2.29 (2.37–2.29)	34.40–2.79 (2.89–2.79)	33.67–2.69 (2.79–2.69)
<i>R</i> _{merge}	0.035 (0.647)	0.055 (0.637)	0.119 (0.557)	0.089 (0.793)	0.088 (0.381)	0.085 (0.394)
<i>I</i> / σ <i>I</i>	7.2 (2.3)	9.7 (1.7)	16.5 (4.0)	21.9 (4.2)	15.5 (4.1)	13.3 (2.6)
Completeness (%)	100.0 (99.9)	94.8 (81.3)	97.6 (95.6)	99.8 (100)	99.5 (99.3)	98.3 (86.3)
Redundancy	6.2 (5.7)	8.0 (4.2)	7.8 (7.4)	11.1 (11.9)	7.0 (7.3)	14.4 (8.0)
Refinement						
Resolution (Å)	2.19	2.39	2.89	2.29	2.79	2.69
No. reflections	28,629	57,397	35,289	23,158	12,680	14,477
<i>R</i> _{work} / <i>R</i> _{free}	0.217/0.255	0.216/0.245	0.215/0.253	0.222/0.258	0.203/0.269	0.216/0.267
No. atoms						
Protein	3,564	7,084	7,145	2,922	2,925	2,931
Heterogen	56	17	30	4	14	14
Water	206	329	166	111	50	38
<i>B</i> -factors (Å ²)						
Protein	25.7	41.0	32.7	42.9	47.3	53.9
H3 peptide	22.1					
Cofactor	32.0	75.5	82.2	57.0	69.3	92.6
Water	29.8	37.5	22.6	47.1	40.7	41.0
R.m.s. deviations						
Bond lengths (Å)	0.006	0.006	0.008	0.009	0.007	0.006
Bond angles (°)	1.2	1.3	1.3	1.4	1.3	1.3

^aValues in parentheses are for highest-resolution shell.

N-oxalylglycine (Fig. 1h). The active site cannot accommodate a trimethylated lysine because the third methyl group would cause repulsive tension with *N*-oxalylglycine. Phe279, substitution of which (to serine) causes inherited X-linked metal retardation^{22–24}, makes van der Waals contacts with Ile248 and Ile318 (Supplementary Fig. 3j), forming a hydrophobic core supporting the backbone of Fe²⁺-coordinating residues His247, Asp249, and His319.

H3K4me3 binding by KIAA1718 PHD inhibits its jumonji activity

Unlike PHF8, KIAA1718 (Fig. 2) is highly active on H3_{1–24}K9me2, with *t*_{1/2} ~ 4 min and *k*_{cat} = 6.5 h^{–1} (Fig. 2a, top panels). Unexpectedly, the presence of both H3K4me3 and H3K9me2 on the same peptide, H3_{1–24}K4me3-K9me2, has exactly the opposite effect on KIAA1718 compared to PHF8: it nearly abolishes the demethylation activity of KIAA1718 on K9me2 (Fig. 2a, lower left). Apparently, binding of the PHD to H3K4me3 (Fig. 2b) prevents demethylation of K9me2 by the linked jumonji domain, which on its own is active on H3K9me2 with *k*_{cat} = 6 h^{–1} and *k*_{cat}/*K*_M = 0.5 h^{–1} μmol^{–1} (Supplementary Fig. 4e). The doubly methylated peptide inhibits KIAA1718 activity on H3_{1–24}K9me2 with a half-maximal inhibitory concentration (IC₅₀) of 3.1 μM (Fig. 2a, lower right) under MS assay conditions (Supplementary Fig. 5).

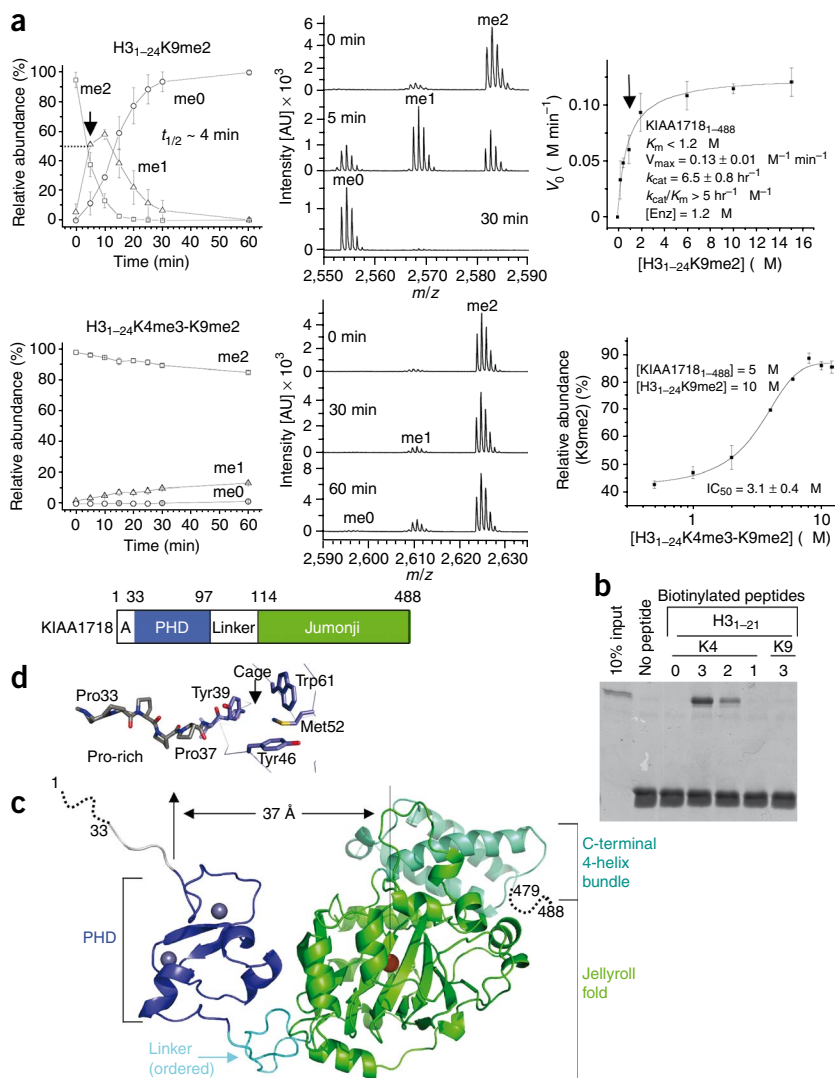
The crystal structure of the apo-form KIAA1718, determined at the resolution of 2.4 Å in the presence of *N*-oxalylglycine (Table 1), suggests a mechanism for this inhibition. Residues 32–479 of KIAA1718 (Fig. 2c) have continuous electron density through the main chain. The disordered residues include the C-terminal tail (residues 480–488) and the N-terminal tail (residues 1–31), the latter of which is absent in the KIAA1718 orthologs of zebrafish and *Xenopus laevis* (Supplementary Fig. 2) and whose deletion has no impact on activity (Supplementary Fig. 6). The six-proline stretch (Pro32–Pro37)

displays an extended conformation (Fig. 2d). An identical surface hydrophobic cage to that of PHF8 is formed by two tyrosines, one tryptophan and one methionine (Fig. 2d). The cage is likely where H3K4me3 would bind, as the PHD alone binds tri- and dimethylated H3K4 peptide (Fig. 2b). Unlike PHF8, the linker between PHD and jumonji (residues 98–113) seems ordered, as indicated by the continuity of electron density and similarity of crystallographic thermal factors for all three regions (25 Å² for PHD, 30 Å² for the linker and 35 Å² for jumonji).

The distance between the PHD cage (the H3K4me3 binding site) and the jumonji Fe²⁺-binding site, immediately adjacent to the presumed target methyl-lysine binding site, is approximately 37 Å (Fig. 2c). This is more than twice the linear distance of ~16 Å between H3K4 and H3K9 in an extended form of the substrate. Isothermal titration calorimetric (ITC) analysis shows that KIAA1718 binds the doubly methylated peptide, H3_{1–24}K4me3-K9me2, with *K*_D ~ 0.3 μM; removing the three methyl groups at H3K4 increased *K*_D to ~60 μM, a reduction by a factor of 200 in binding affinity (Fig. 3a). Therefore, the dominating interaction between KIAA1718 and the doubly methylated peptide is the binding of H3K4me3 by the PHD. This interaction would place H3K9me2 too far from the active site of the linked jumonji domain in this extended conformation.

The individual domain structures of KIAA1718 and PHF8 are very similar, with an r.m.s. deviation of less than 0.65 Å when comparing the 58 pairs of PHD C α atoms and less than 0.89 Å when comparing the 361 pairs of jumonji C α atoms. Superimposition of the two enzymes by their jumonji domains reveals that the PHF8 PHD adopts a bent conformation toward the jumonji domain in the presence of substrate binding, whereas the PHD and jumonji domains of KIAA1718 adopt an extended conformation in its apo structure with an ordered linker (Fig. 3b).

Figure 2 KIAA1718 PHD binding of H3K4me3 inhibits its jumonji domain activity targeting H3K9me2. (a) Effect of H3K4me3 on the demethylation of H3K9me2 by KIAA1718. Left panels show progression of demethylation as a function of reaction time. Middle panels show representative mass spectra at various time points. Right top panel shows kinetics of KIAA1718 on substrate H₃₁₋₂₄K9me2. K_M is estimated to be less than 1.2 μ M (indicated by an arrow), which is the amount of enzyme used to generate sufficient fluorescence signal. Right bottom shows the IC_{50} value of H₃₁₋₂₄K4me3-K9me2 peptide [I] on H₃₁₋₂₄K9me2 [S] demethylase activity of KIAA1718 [E]. The relative abundance of the substrate [S] was measured after eight minutes incubation at 37 °C by adding varying amounts of [I] to the reaction mixture. No demethylation of the doubly methylated peptide occurred. (b) Peptide pull-down assays with peptides H₃₁₋₂₁ that were unmodified or mono-, di- or trimethylated (1, 2 or 3) at H3K4 or H3K9 using a GST-tagged PHD domain of KIAA1718. (c) KIAA1718 contains four segments: a disordered alanine-rich sequence followed by a stretch of prolines, a PHD domain (blue) containing two zinc metals (gray balls), a rigid linker (cyan) and a jumonji domain (green) followed by a four-helix bundle. (d) The KIAA1718 PHD domain contains a surface hydrophobic cage, a presumptive site for binding of H3K4me3. In the crystal lattice, the cage is blocked by the N-terminal prolines of a crystallographic symmetry-related molecule (**Supplementary Fig. 6c**).



To test the idea that the linkers are critical determinants of demethylase activity, we engineered two hybrid enzymes: KIAA1718 carrying the PHF8 linker and PHF8 carrying the KIAA1718 linker (**Fig. 3c** and **Supplementary Fig. 7a**). Notably, the hybrid enzymes lost their parental features and became indistinguishable; both were equally active on doubly methylated H₃₁₋₂₄K4me3-K9me2 and had a less than two-fold difference of activity on H₃₁₋₂₄K9me2 (**Supplementary Fig. 7b**). Compared to the wild-type enzymes, the most noteworthy change was in the substantial gain of activity by the KIAA1718-PHF8 linker hybrid on H₃₁₋₂₄K4me3-K9me2 with $t_{1/2} = 9$ min (**Fig. 3c**, right graph), in stark contrast to the barely detectable activity of native KIAA1718 on the same peptide (see **Fig. 2a**, lower left). We thus conclude that the PHF8 linker in the hybrid enzyme enables the PHD and jumonji domains to adopt a closed conformation just like the native PHF8, whereas the native KIAA1718 locks the two domains in an extended conformation.

KIAA1718 demethylates H3K27me2 in the presence of H3K4me3

We modeled a H3K4me3 peptide onto KIAA1718-PHD and a H3K9me2 peptide onto KIAA1718-jumonji by superimposing the portions of H3 peptide bound to the PHF8-PHD and PHF8-jumonji domains, respectively (**Fig. 4a**). The adoption of an extended conformation by KIAA1718 suggests that a peptide carrying H3K4me3 and H3K27me2 (which shares an ARKS tetrapeptide sequence with that of H3K9) could occupy both the PHD and jumonji domains simultaneously and could be demethylated by KIAA1718 in this extended conformation. Indeed, the presence of trimethylated H3K4 enhanced KIAA1718 activity on H3K27me2 by a factor of about 2 ($t_{1/2} = 10$ min

versus 19 min; **Fig. 4b**), in contrast to the severe inhibition of H3K9me2 demethylation (see **Fig. 2a**, lower left). Moreover, in a reaction mixture containing the two substrates in equimolar ratio, KIAA1718 selectively demethylated the peptide containing both H3K4me3 and H3K27me2 (**Fig. 4c**). This is consistent with the notion that PHD preferentially bound H3K4me3 first and subsequently allowed only H3K27me2 on the same peptide to be demethylated by the jumonji domain.

DISCUSSION

Here we show, enzymatically and structurally, that the PHDs of PHF8 and KIAA1718 bind H3K4me3—a modification associated with transcriptional activation, as their linked jumonji domains remove methyl marks from H3K9 (PHF8) and H3K27 (KIAA1718) that are associated with transcriptional repression. These opposing marks (one for activation and the other for repression) do sometimes coexist, particularly colocalization of H3K27me to genes that are H3K4me modified^{26–29}. We hypothesize that, *in vivo*, PHF8 and KIAA1718 are recruited to H3K4me3 marks via their PHDs, and that subsequently the jumonji domain amplifies this activating signal by removing any local repressing methyl groups (**Supplementary Fig. 8a**). In PHF8 the shorter and perhaps more flexible linker between the PHD and jumonji domains enables the active site of jumonji to reach the target H3K9me2 while the PHD binds to H3K4me3.

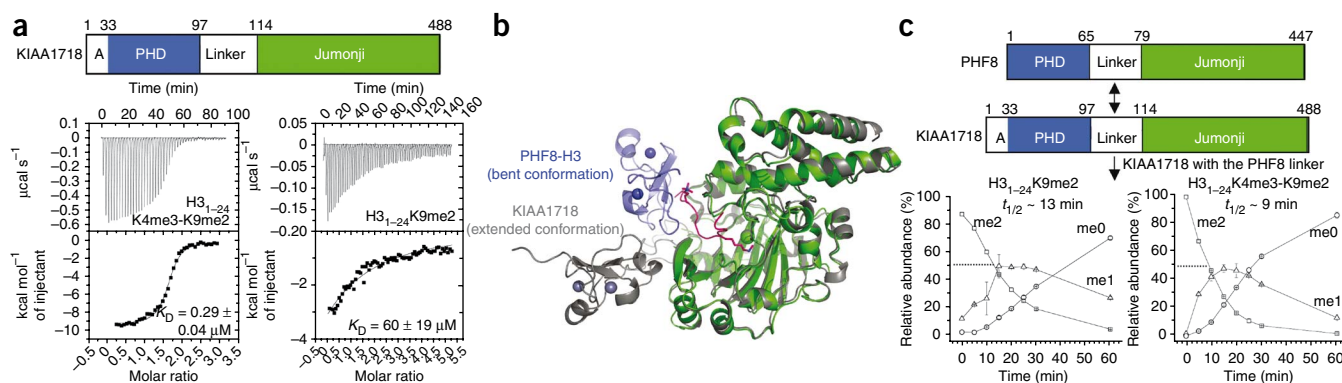


Figure 3 Effect of the linker on the KIAA1718 jumonji activity targeting H3K9me2. **(a)** ITC measurements of binding of the KIAA1718 to doubly methylated H₃₁₋₂₄K4me3-K9me2 peptides (left) and H₃₁₋₂₄K9me2 peptides (right). The measurements were carried out under the conditions of 18 μ M protein concentration and 0.4 mM peptide concentration in 50 mM NaCl and 50 mM HEPES, pH 7.0. **(b)** Superimposition of PHF8 (colored) and KIAA1718 (gray) in their respective jumonji domains. **(c)** The engineered hybrid enzyme of KIAA1718 carrying the PHF8 linker gains substantial activity on H₃₁₋₂₄K3me3-K9me2 (right), faster by a factor of more than 100 than that of the wild-type enzyme (see Fig. 2a).

The binding of substrate together by both domains makes the H3K4me3-H3K9me2 a better substrate for PHF8 (higher k_{cat}/K_M). In contrast, the corresponding ordered linker in KIAA1718 renders the enzyme inactive on H3K9me2 when H3K4me3 is present, in the process becoming more selective toward H3K27me2 (Supplementary Fig. 8b). We conclude that the structural linkage between the PHD binding to H3K4me3 and the placement of the catalytic jumonji domains relative to this 'ON', or active, epigenetic landmark determines which repressive marks are removed in both demethylases.

It remains to be tested whether KIAA1718 also becomes more active or inhibited on H3K36me2 (ref. 21) when H3K4me3 is present on the same peptide (Supplementary Fig. 9). It is also interesting to note that PHF8₁₋₄₄₇ is nearly inactive on H3K27me2 and H3K36me2 under the conditions tested (Supplementary Fig. 10a). However, a truncated protein with the PHD deleted, PHF8₆₂₋₄₄₇, has weak activity on H3K27me2 and H3K36me2 (Supplementary Fig. 10b), suggesting that the linked PHD (probably in the closed conformation) can interfere with substrate access to jumonji domain. Taking these results together, we suggest that the PHF8 and KIAA1718 jumonji domains on their own are promiscuous enzymes; it is the associated PHDs and the linker—a determinant for the relative positioning of the two domains—that are mainly responsible for substrate specificity.

The successful generation of hybrid enzymes may lead to a way to engineer enzymes with novel specificities by fusing an epigenetic reader (for highly specific binding of methyl-lysine or acetyl-lysine or other modifications) and a promiscuous enzymatic jumonji domain via a variable linker. Such enzymes could be useful tools *in vitro* and *in vivo* for the study of combinations of histone modifications.

The existence of combinatorial readout of multiple covalent histone modifications is an explicit prediction of the 'histone code hypothesis'³⁰⁻³³. Binding of substrate using two or more domains in concert to enhance an enzyme's activity and its substrate specificity may be a general mechanism for jumonji-containing protein lysine demethylases. For example, JHDM2A-mediated demethylation of histone H3K9me1 or H3K9me2 requires a zinc finger located N-terminally to the jumonji domain for JHDM2A's enzymatic activity⁵. JARID jumonji family proteins contain a jumonji domain that demethylates H3K4me3 surrounded by several PHDs, and at least one of them binds H3K9me3 (refs. 34,35) (Supplementary Fig. 8c). Mutation or deletion of this PHD impairs the demethylase activity on H3K4me3 (refs. 34,35). Several histone-methylating enzymes contain components (domains) to both synthesize and bind a specific histone mark, for example mammalian G9a/GLP (for H3K9me1 and H3K9me2) (ref. 36) and *Schizosaccharomyces pombe* Clr4

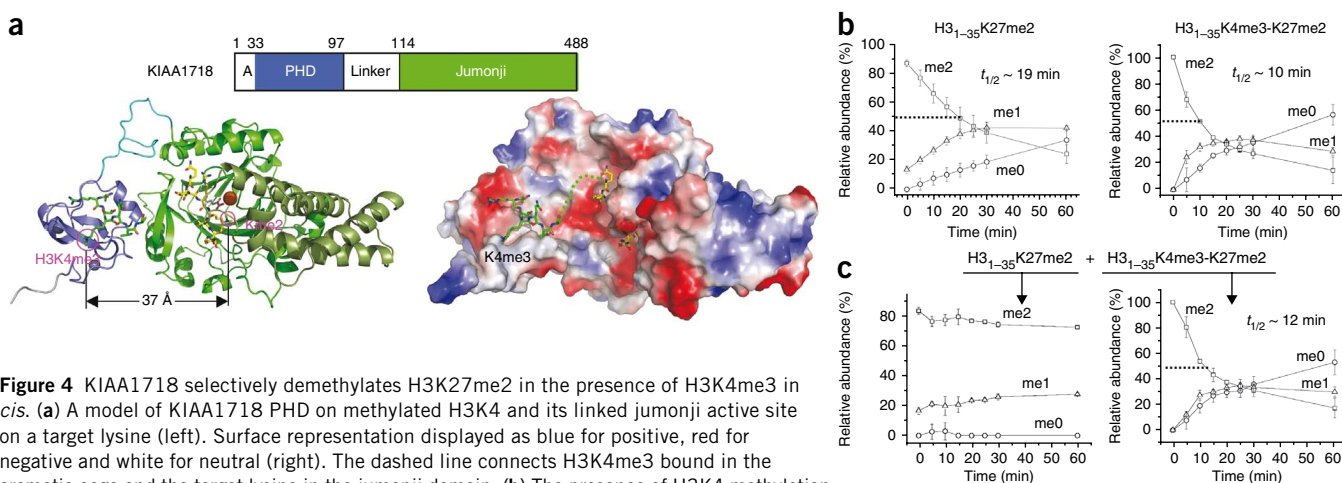


Figure 4 KIAA1718 selectively demethylates H3K27me2 in the presence of H3K4me3 in *cis*. **(a)** A model of KIAA1718 PHD on methylated H3K4 and its linked jumonji active site on a target lysine (left). Surface representation displayed as blue for positive, red for negative and white for neutral (right). The dashed line connects H3K4me3 bound in the aromatic cage and the target lysine in the jumonji domain. **(b)** The presence of H3K4 methylation in *cis* enhances KIAA1718 demethylase activities on H3K27me2. **(c)** When two peptide substrates were mixed in equimolar ratio, H₃₁₋₃₅K27me2 (left) and H₃₁₋₃₅K4me3-K27me2 (right), KIAA1718 selectively demethylated H₃₁₋₃₅ peptides containing both H3K4me3 and H3K27me2 (right).

(for H3K9me3) (ref. 37). They contain modules within the same polypeptide for both making (via the SET domain) and recognizing (via the ankyrin repeats or chromodomain) a given methyl mark; a mechanism of cross-talk propagates a given methyl mark. PHF8 and KIAA1718 contain modules within the same polypeptide for both recognizing (via the PHD) and removing (via the jumonji domain) two opposing methyl marks—a mechanism of cross-talk removes an ‘OFF’ methyl mark based on an existing ‘ON’ methyl mark. Understanding the function and cross-talk of individual ‘letters’ (one methyl mark, two methyl marks, and so on) will eventually allow researchers to uncover the complex language of the histone code^{30,38}.

METHODS

Methods and any associated references are available in the online version of the paper at <http://www.nature.com/nsmb/>.

Accession codes. Protein Data Bank: The coordinates and structure factors have been deposited with accession numbers 3KV4 (for PHF8_{1–447}), 3KV5 and 3KV6 (for KIAA1718_{1–488}) and 3KV9, 3KVA and 3KVB (for KIAA1718_{92–488}), respectively.

Note: Supplementary information is available on the Nature Structural & Molecular Biology website.

ACKNOWLEDGMENTS

We thank A. Ruiz and R. Gridds for technical assistance, R.M. Blumenthal for critical comments, A.S. Bhagwat and T.W. Roy (Wayne State University) for *Escherichia coli* strain BH249 overexpressing formaldehyde dehydrogenase and T. Kutateladze (University of Colorado) and A. Mattevi and C. Binda (University of Pavia) for H3K4me3-containing peptides. The Department of Biochemistry at the Emory University School of Medicine supported the use of the SER-CAT synchrotron beamline at the Advanced Photon Source of Argonne National Laboratory, local X-ray facility and MALDI-TOF mass spectrometry. This work was supported by grants GM06860 and DK082678 to X.C. and GM058012 and NCI18487 to Y.S. from the US National Institutes of Health. Y.S. is a cofounder of Constellation Pharmaceutical. X.C. is a Georgia Research Alliance Eminent Scholar.

AUTHOR CONTRIBUTIONS

J.R.H. performed crystallographic experiments; A.K.U. performed kinetic experiments; H.H.Q. and Y.S. provided initial expression constructs and the knowledge of specificities of individual PHD and jumonji domains; X.Z. generated hybrid enzymes; X.C. organized and designed the scope of the study and wrote the manuscript, and all others helped in analyzing data and revising the manuscript.

Published online at <http://www.nature.com/nsmb/>.

Reprints and permissions information is available online at <http://npg.nature.com/reprintsandpermissions/>.

1. Rea, S. *et al.* Regulation of chromatin structure by site-specific histone H3 methyltransferases. *Nature* **406**, 593–599 (2000).
2. van Leeuwen, F., Gafken, P.R. & Gottschling, D.E. Dot1p modulates silencing in yeast by methylation of the nucleosome core. *Cell* **109**, 745–756 (2002).
3. Shi, Y. *et al.* Histone demethylation mediated by the nuclear amine oxidase homolog LSD1. *Cell* **119**, 941–953 (2004).
4. Tsukada, Y. *et al.* Histone demethylation by a family of JmjC domain-containing proteins. *Nature* **439**, 811–816 (2006).
5. Yamane, K. *et al.* JHDM2A, a JmjC-containing H3K9 demethylase, facilitates transcription activation by androgen receptor. *Cell* **125**, 483–495 (2006).
6. Whetstone, J.R. *et al.* Reversal of histone lysine trimethylation by the JMJD2 family of histone demethylases. *Cell* **125**, 467–481 (2006).
7. Wysocka, J. *et al.* PHD finger of NURF couples histone H3 lysine 4 trimethylation with chromatin remodelling. *Nature* **442**, 86–90 (2006).

8. Li, H. *et al.* Molecular basis for site-specific readout of histone H3K4me3 by the BPTF PHD finger of NURF. *Nature* **442**, 91–95 (2006).
9. Shi, X. *et al.* ING2 PHD domain links histone H3 lysine 4 methylation to active gene repression. *Nature* **442**, 96–99 (2006).
10. Pena, P.V. *et al.* Molecular mechanism of histone H3K4me3 recognition by plant homeodomain of ING2. *Nature* **442**, 100–103 (2006).
11. Lan, F. *et al.* Recognition of unmethylated histone H3 lysine 4 links BHC80 to LSD1-mediated gene repression. *Nature* **448**, 718–722 (2007).
12. Ooi, S.K.T. *et al.* DNMT3L connects unmethylated lysine 4 of histone H3 to de novo methylation of DNA. *Nature* **448**, 714–717 (2007).
13. Klöse, R.J., Kallin, E.M. & Zhang, Y. JmjC-domain-containing proteins and histone demethylation. *Nat. Rev. Genet.* **7**, 715–727 (2006).
14. Couture, J.F., Collazo, E., Ortiz-Tello, P.A., Brunzelle, J.S. & Trievel, R.C. Specificity and mechanism of JMJD2A, a trimethyllysine-specific histone demethylase. *Nat. Struct. Mol. Biol.* **14**, 689–695 (2007).
15. Ng, S.S. *et al.* Crystal structures of histone demethylase JMJD2A reveal basis for substrate specificity. *Nature* **448**, 87–91 (2007).
16. Chen, Z. *et al.* Structural basis of the recognition of a methylated histone tail by JMJD2A. *Proc. Natl. Acad. Sci. USA* **104**, 10818–10823 (2007).
17. Huang, Y., Fang, J., Bedford, M.T., Zhang, Y. & Xu, R.M. Recognition of histone H3 lysine-4 methylation by the double tudor domain of JMJD2A. *Science* **312**, 748–751 (2006).
18. Lee, J., Thompson, J.R., Botuyan, M.V. & Mer, G. Distinct binding modes specify the recognition of methylated histones H3K4 and H4K20 by JMJD2A-tudor. *Nat. Struct. Mol. Biol.* **15**, 109–111 (2008).
19. Fatemi, M., Hermann, A., Pradhan, S. & Jeltsch, A. The activity of the murine DNA methyltransferase Dnmt1 is controlled by interaction of the catalytic domain with the N-terminal part of the enzyme leading to an allosteric activation of the enzyme after binding to methylated DNA. *J. Mol. Biol.* **309**, 1189–1199 (2001).
20. Pradhan, M. *et al.* CXXC domain of human DNMT1 is essential for enzymatic activity. *Biochemistry* **47**, 10000–10009 (2008).
21. Loenarz, C. *et al.* PHF8, a gene associated with cleft lip/palate and mental retardation, encodes for an N^ε-dimethyl lysine demethylase. *Hum. Mol. Genet.* Published online, doi:10.1093/hmg/ddp480 (19 October 2009).
22. Abidi, F.E., Miano, M.G., Murray, J.C. & Schwartz, C.E. A novel mutation in the PHF8 gene is associated with X-linked mental retardation with cleft lip/cleft palate. *Clin. Genet.* **72**, 19–22 (2007).
23. Koivisto, A.M. *et al.* Screening of mutations in the PHF8 gene and identification of a novel mutation in a Finnish family with XLMR and cleft lip/cleft palate. *Clin. Genet.* **72**, 145–149 (2007).
24. Laumonnier, F. *et al.* Mutations in PHF8 are associated with X-linked mental retardation and cleft lip/cleft palate. *J. Med. Genet.* **42**, 780–786 (2005).
25. Couture, J.F., Hauk, G., Thompson, M.J., Blackburn, G.M. & Trievel, R.C. Catalytic roles for carbon-oxygen hydrogen bonding in SET domain lysine methyltransferases. *J. Biol. Chem.* **281**, 19280–19287 (2006).
26. Bernstein, B.E. *et al.* Genomic maps and comparative analysis of histone modifications in human and mouse. *Cell* **120**, 169–181 (2005).
27. Azuara, V. *et al.* Chromatin signatures of pluripotent cell lines. *Nat. Cell Biol.* **8**, 532–538 (2006).
28. Zhao, X.D. *et al.* Whole-genome mapping of histone H3 Lys4 and 27 trimethylations reveals distinct genomic compartments in human embryonic stem cells. *Cell Stem Cell* **1**, 286–298 (2007).
29. Pan, G. *et al.* Whole-genome analysis of histone H3 lysine 4 and lysine 27 methylation in human embryonic stem cells. *Cell Stem Cell* **1**, 299–312 (2007).
30. Strahl, B.D. & Allis, C.D. The language of covalent histone modifications. *Nature* **403**, 41–45 (2000).
31. Jenuwein, T. & Allis, C.D. Translating the histone code. *Science* **293**, 1074–1080 (2001).
32. Turner, B.M. Defining an epigenetic code. *Nat. Cell Biol.* **9**, 2–6 (2007).
33. Sugauma, T. & Workman, J.L. Crosstalk among histone modifications. *Cell* **135**, 604–607 (2008).
34. Iwase, S. *et al.* The X-linked mental retardation gene SMCX/JARID1C defines a family of histone H3 lysine 4 demethylases. *Cell* **128**, 1077–1088 (2007).
35. Li, F. *et al.* Lid2 is required for coordinating H3K4 and H3K9 methylation of heterochromatin and euchromatin. *Cell* **135**, 272–283 (2008).
36. Collins, R.E. *et al.* The ankyrin repeats of G9a and GLP histone methyltransferases are mono- and dimethyllysine binding modules. *Nat. Struct. Mol. Biol.* **15**, 245–250 (2008).
37. Zhang, K., Mosch, K., Fischle, W. & Grewal, S.I. Roles of the Clr4 methyltransferase complex in nucleation, spreading and maintenance of heterochromatin. *Nat. Struct. Mol. Biol.* **15**, 381–388 (2008).
38. Berger, S.L. The complex language of chromatin regulation during transcription. *Nature* **447**, 407–412 (2007).



ONLINE METHODS

We purified GST fusion proteins containing residues for KIAA1718₁₋₄₈₈ (pXC720), KIAA1718₃₈₋₄₈₈, KIAA1718₉₂₋₄₈₈, PHF8₁₋₄₄₇ (pXC721) and PHF8₆₂₋₄₄₇ via three-column chromatography. We solved the structures by molecular replacement. We conducted demethylation assays using MS- and fluorescence-based approaches.

Peptide synthesis. We synthesized peptides H3₁₋₁₅K9me2, H3₁₋₂₄K9me2 and H3₁₋₂₄K4me3-K9me2 at the W.M. Keck Foundation Biotechnology Resource Laboratory (Yale University). We synthesized peptides H3₁₋₃₅K27me2 and H3₁₋₃₅K4me3-K27me2 (small amounts) from 21st Century Biochemicals. Peptides H3₁₋₁₂K4me3 and H3₁₋₂₁K4me3 were gifts from T. Kutateladze and from A. Mattevi and C. Binda, respectively.

Protein purification and crystallography. We expressed GST fusion proteins containing residues for KIAA1718₁₋₄₈₈, KIAA1718₉₂₋₄₈₈ and PHF8₁₋₄₄₇ in BL21(DE3)CodonPlus cells using autoinduction³⁹. We expressed KIAA1718 protein at 37 °C and PHF8 at 16 °C, and we induced the latter with 0.4 mM isopropyl β-D-thiogalactoside in autoinduction medium without lactose. We purified both proteins using GST affinity (while the fusion protein was still on the column, the GST-tagged proteins were cleaved with thrombin for either 1 or 2 h at room temperature (~21 °C) or overnight (~16 h) at 4 °C), HiTrapSP and S75 Sepharose sizing columns (GE Healthcare). We concentrated the proteins to approximately 20 mg ml⁻¹ in 20 mM bis-Tris, pH 5.5, 200 mM NaCl, 5% (v/v) glycerol and 1 mM DTT. We added cofactor α-ketoglutarate (Sigma-Aldrich) or its analog N-oxalylglycine (Alexis Biochemicals) and in some preparations metal ions shortly before crystallization to 5–10 mM FeCl₂ or 1–4 mM NiCl₂ concentration.

We obtained KIAA1718₁₋₄₈₈ crystals under the conditions of 5–10% (v/v) polyethylene glycol 3350, 0.2 M potassium thiocyanate and 0.1 M bis-Tris, pH 6.0. We collected two data sets, one at 2.4-Å resolution in the presence of N-oxalylglycine and the other at 2.9-Å resolution in the presence of α-ketoglutarate (Table 1). We used the molecular replacement program PHASER⁴⁰ to obtain crystallographic phases. For KIAA1718, we generated the initial search models for jumonji domain and PHD, respectively, using the PHYRE server⁴¹ (<http://www.sbg.bio.ic.ac.uk/phyre/index.cgi>), primarily based on the structure of human JHDM1A jumonji domain⁴² (PDB 2YU2) and the NMR structure of PHF8 (He, E, Inoue, M., Kigawa, T., Shirouzu, M., Terada, T., Muto, Y. & Yokoyama, S., unpublished results) (PDB 1WEP). The resulting electron density map for the linker region between the two domains was easily traced.

In addition, we solved structures of the KIAA1718 jumonji domain (residues 92–488) in three forms, in the absence and presence of cofactor α-ketoglutarate or N-oxalylglycine (Table 1). The fragment is active on H3K9me2, H3K27me2 and H3K36me2 (Supplementary Fig. 12). We obtained KIAA1718₉₂₋₄₈₈ crystals under conditions using 17–20% (v/v) polyethylene glycol 5000 monomethyl ether, 0.2 M CaCl₂ and 0.1 M bis-Tris, pH 6.4. We determined the structures in the resolution range of 2.3–2.8 Å. The N-terminal residues (92–113) including the linker were disordered in the absence of the PHD domain.

We obtained the PHF8 crystals with H3₁₋₂₄K4me3-K9me2 peptide under conditions of 25% (v/v) polyethylene glycol 3350, 0.2 M NaCl, and 0.1 M sodium citrate, pH 5.6, with a peptide-to-protein ratio of 2:1. We transferred the crystals to a solution containing 20% (v/v) ethylene glycol and 2 mM N-oxalylglycine before flash freezing them in liquid nitrogen and using them for data collection. The X-ray diffraction data of PHF8-peptide complexes were collected from a crystal at the resolution of 2.2 Å (Table 1). For molecular replacement, the PHD and jumonji domains of KIAA1718 were used separately as search models. The resulting electron density map for peptide was easily identified, including H3K4me3 and H3K9me2 (Fig. 1e). The electron density map was sufficient to distinguish unambiguously 14 residues (1–14) of the histone H3 peptide with a less ordered H3K14 side chain (Supplementary Fig. 3k). We used the graphic model building programs O⁴³ and Coot⁴⁴ and the refinement program CNS⁴⁵. We collected all X-ray diffraction data at APS SERCAT beamlines (22-ID or 22-BM). We used the program MacPyMol (DeLano Scientific) to generate structural figures.

MS-based demethylation assay. We probed time courses of demethylation reactions using a MALDI-TOF MS-based assay using a Burkert Ultra FlexII TOF/TOF instrument (Biochemistry Department, Emory University). Briefly, we incubated differentially methylated histone H3 peptide substrates with purified proteins at

37 °C in 50 mM HEPES, pH 7.0, reaction buffer containing 50 μM (NH₄)₂FeSO₄, 1 mM α-ketoglutarate and 2 mM ascorbic acid. For all reactions, we maintained substrate peptide concentrations at 10 μM and protein concentrations at 5 μM. We withdrew an aliquot of 1 μl reaction mixture at the desired time point and mixed it with 4 μl of 50% (v/v) acetonitrile and 0.1% (v/v) trifluoroacetic acid (TFA). We spotted an aliquot of 1 μl of this mixture on the MALDI target plate together with 1 μl of α-cyano-4-hydroxycinnamic acid (CHCA) matrix solution (10 mg ml⁻¹) in 50% (v/v) acetonitrile, 0.1% (v/v) TFA. We recorded all mass spectra in reflection mode by averaging over more than ten different points in the sample spot (examples shown in Fig. 2b middle panels for KIAA1718 and Supplementary Fig. 11a for PHF8).

Fluorescence-based demethylation assay. We determined kinetic parameters of demethylation reactions based on a formaldehyde dehydrogenase (FDH)-coupled continuous fluorescent assay⁴⁶. Reactions were carried out at 37 °C in 50 mM HEPES, pH 7.0, buffer containing 50 μM (NH₄)₂FeSO₄, 1 mM α-ketoglutarate and 2 mM ascorbic acid, 1 mM 3-acetylpyridine adenine dinucleotide (APAD⁺) (Sigma) and 0.05 units of FDH, the latter of which were purified from *E. coli* strain BH249 (a gift from A.S. Bhagwat and T.W. Roy). We carried out all reactions by preincubating the enzyme for 30 min at room temperature in the reaction mixture and then adding desired amount of peptide substrate to start the reaction. We monitored the rate of demethylation by measuring the rate of oxidation of formaldehyde to formic acid by FDH, which reduces APAD⁺ (a more stable analog of NAD⁺)⁴⁶ to APADH. We followed the reactions at an excitation wavelength of 363 nm and an emission wavelength of 482 nm on an AMINCO-Bowman Series 2 spectrofluorometer (Thermo Electron Scientific Instruments Corporation) equipped with a thermostatable cuvette holder. We calibrated fluorescence intensities against samples with known formaldehyde concentrations (Supplementary Fig. 4). We calculated the initial velocities from the slopes and plotted against substrate concentrations. We calculated the kinetic parameters by fitting the data to the Michaelis-Menten equation using Origin 6.0. We performed all reactions in triplicate.

ITC measurements. We carried out ITC measurements using an enzyme concentration of 11 μM (or 18 μM) with 0.2 mM (or 0.4 mM) peptide concentration in 100 mM (or 50 mM) NaCl and 50 mM HEPES, pH 7.0, on a MicroCal VP-ITC instrument at 25 °C. We calculated binding constants by fitting the data using the ITC data-analysis module of Origin 7.0 (OriginLab Corporation).

Engineering hybrid enzymes. We constructed the vectors for producing hybrid enzymes by overlapping PCR. For the KIAA1718 with the PHF8 linker, we used primers containing either strand of the entire PHF8 linker (33 nt) followed by KIAA1718 sequences flanking either side of the linker to PCR the PHD domain or jumonji domain (when paired with vector primers). We purified the resulting products, annealed them and reamplified them with vector primers to generate hybrid DNA and cloned them into the pGEX vector. For the PHF8 with the KIAA1718 linker, we used partial KIAA1718 linker sequences (with a 33-nt overlap) as primers. We sequenced the hybrids to verify the presence of the intended linker. We expressed and purified the hybrid enzymes in ways similar to those used for the wild-type enzymes.

39. Studier, F.W. Protein production by auto-induction in high density shaking cultures. *Protein Expr. Purif.* **41**, 207–234 (2005).
40. Storoni, L.C., McCoy, A.J. & Read, R.J. Likelihood-enhanced fast rotation functions. *Acta Crystallogr. D Biol. Crystallogr.* **60**, 432–438 (2004).
41. Kelley, L.A., MacCallum, R.M. & Sternberg, M.J. Enhanced genome annotation using structural profiles in the program 3D-PSSM. *J. Mol. Biol.* **299**, 499–520 (2000).
42. Han, Z., Liu, P., Gu, L., Zhang, Y., Chen, S. & Chai, J. Structure basis for histone demethylation by JHDM1. *Frontier Science* **1**, 52–67 (2007).
43. Jones, T., Zou, J.Y., Cowan, S.W. & Kjeldgaard, M. Improved methods for building protein models in electron density maps and the location of errors in these models. *Acta Crystallogr. A* **47**, 110–119 (1991).
44. Emsley, P. & Cowtan, K. Coot: model-building tools for molecular graphics. *Acta Crystallogr. D Biol. Crystallogr.* **60**, 2126–2132 (2004).
45. Brunger, A.T. *et al.* Crystallography & NMR system: A new software suite for macromolecular structure determination. *Acta Crystallogr. D Biol. Crystallogr.* **54**, 905–921 (1998).
46. Roy, T.W. & Bhagwat, A.S. Kinetic studies of *Escherichia coli* AlkB using a new fluorescence-based assay for DNA demethylation. *Nucleic Acids Res.* **35**, e147 (2007).